J. Fluid Mech. (1971), *vol.* 49, *part* 2, *pp.* 327–336
Printed in Great Britain

A model for the boundary condition of a porous material. Part 2

By S. RICHARDSON

Department of Applied Mathematics and Theoretical Physics,
University of Cambridge

(Received 20 December 1970)

The present paper contains an analysis of the model of a porous material proposed in part 1, and carries out calculations which allow comparison between theory and the experiments described therein. The relevant boundary conditions to be applied at an interface between a fluid and such a material are considered.

1. Introduction and basic equations

We consider the flow produced above a corrugated surface by a plane surface moving parallel to the corrugations at a fixed distance from it. Take rectangular Cartesian co-ordinates (x, y, z), with the x axis in the direction of the motion and the corrugations. Writing $z = x + iy$ and assuming a symmetry and a periodicity in the geometry in the direction perpendicular to the motion, we have the situation sketched in the z plane of figure 1.

There is just one velocity component, u, in the x direction which is harmonic and, therefore, expressible as $u = \mathrm{Re}\{\phi(z)\}$ where $\phi(z)$ is an analytic function of z in the flow domain. By the periodicity we can consider just the region bounded by $ABDC$ in the figure, provided we ensure that u attains equal values at corresponding points of AC and BD. On AB, $u = U$ while on CD, $u = 0$.

The quantity of interest in the present context is the total force, F, exerted on the portion AB of the plane, per unit length in the x direction, and this is

$$F = \mu \int_A^B \frac{\partial u}{\partial y} dx = i\mu \int_A^B \phi'(z)\, dz = i\mu [\phi(z)]_A^B, \tag{1.1}$$

where $[\,]_A^B$ denotes the change in the bracketed quantity in moving from A to B.

The flow domain may be mapped onto the interior of a rectangle in the ζ plane, the points A, B, D, C going to the vertices $-1+ic$, $+1+ic$, $+1$, -1 respectively, as in figure 1, by $z = f(\zeta)$, where $f(\zeta)$ is analytic in the interior. We use the same letters for corresponding points in the different planes throughout the analysis. Defining $\Phi(\zeta) = \phi(f(\zeta))$, the real part of this function takes the value U on AB, zero on CD, and takes equal values at points with equal ordinates on AC and BD (by the symmetry). The solution here is thus $\Phi(\zeta) = -iU\zeta/c$, whence

$$F = 2\mu U/c. \tag{1.2}$$

Thus the required force is determined by a simple geometric property; we conformally map the flow domain onto a rectangle with $ABDC$ going to the vertices,

and the ratio of the sides then gives the results immediately. Using the standard nomenclature of function theory, $\frac{1}{2}c$ is the extremal length of the set of curves in the domain which join AB to CD.

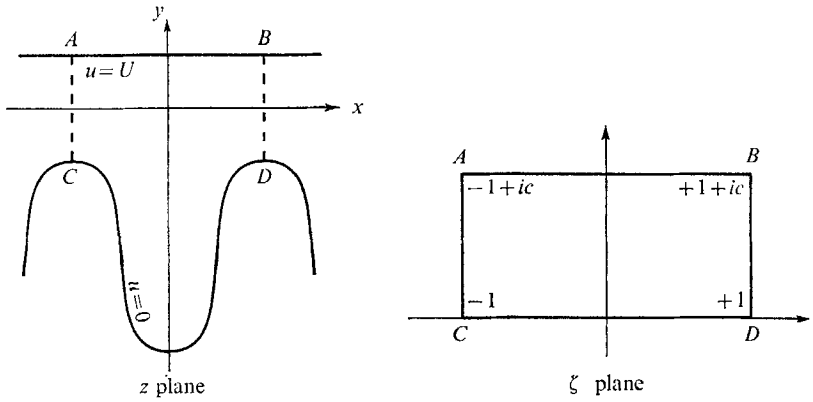

FIGURE 1. z plane and ζ plane for the general problem.

2. Analysis for a grooved plate

Consider now the particular case when the flow region $ABDC$ has the form of the z plane of figure 2. This corresponds to a lower surface consisting of infinitely deep grooves of width s, separated by a distance t, in a flat plate, and differs from the geometry used in the experiments of part 1 only in the infinite depth of the grooves. The actual experiment used grooves whose depth-to-width ratio was 4, but it is shown in the appendix that the error involved in this simplification is negligible. The gap between the plates is denoted by g.

The mean force per unit area of plate is

$$\frac{F}{t+s} = \frac{2\mu U}{c(t+s)}.$$

In the experiment, with the disk of radius R rotating at angular velocity Ω, we therefore expect the disk to experience a torque of magnitude

$$G = \frac{4\pi\mu\Omega}{c(t+s)}\int_0^R r^3 dr = \frac{\pi\mu\Omega R^4}{c(t+s)}, \tag{2.1}$$

the transition from the linear model to the circular motion being valid for $t+s \ll R$ and negligible inertia forces. Thus the geometric parameter, c, is related to the torque by

$$\frac{1}{c} = \frac{(t+s)\,G}{\pi\mu\Omega R^4}. \tag{2.2}$$

The particular geometry of the z plane in figure 2 has been considered by Cockcroft (1927) in the context of an electrostatic problem, but the details are not pursued sufficiently far there for our purposes. In order to maintain the notation adopted by Beavers & Joseph (1967) and used in part 1, with k the Darcy constant and α the dimensionless quantity appearing in the boundary conditions,

it is necessary to adopt a slightly non-standard convention for the elliptic functions. We use the Jacobian elliptic functions $\operatorname{sn} v = \operatorname{sn}(v; l)$, $\operatorname{cn} v = \operatorname{cn}(v; l)$ and $\operatorname{dn} v = \operatorname{dn}(v; l)$ of modulus l, where l is real and $0 \leqslant l \leqslant 1$; the complementary modulus $l' = (1-l^2)^{\frac{1}{2}}$; the complete elliptic integral $K(l)$ and its complement $K'(l) = K(l')$; the elliptic integral of the third kind in Jacobi's form $\Pi(v, \beta) = \Pi(v, \beta; l)$; Jacobi's zeta function $Z(v) = Z(v; l)$ and Jacobi's theta function $\Theta(v) = \Theta(v; l)$. The requisite definitions and properties of these functions can be found in Cayley (1895), Copson (1935) or Milne-Thomson (1950). Whenever the modulus is omitted it is understood to be l.

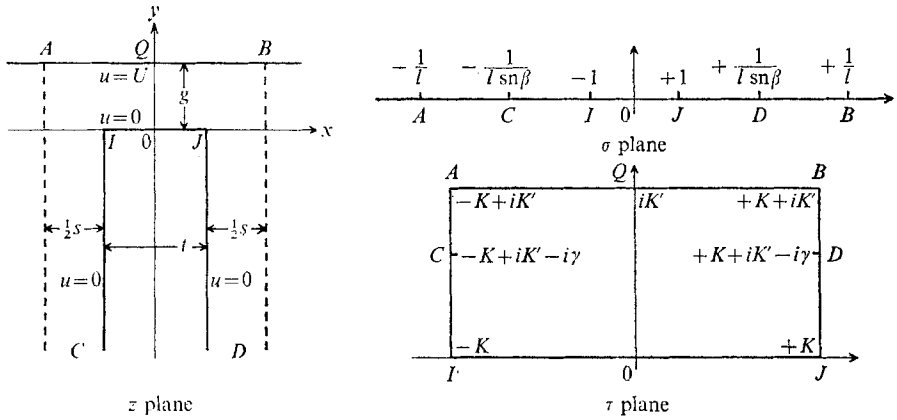

FIGURE 2. z plane, σ plane and τ plane for the particular geometry analysed.

By means of the Schwarz–Christoffel transformation

$$z = H\int_0^{\sigma} \left(\frac{1-\sigma^2}{1-l^2\sigma^2}\right)^{\frac{1}{2}} \frac{d\sigma}{1-l^2\sigma^2\operatorname{sn}^2\beta}, \tag{2.3}$$

where H is a real constant, the z plane of figure 2 is mapped onto the upper half of the σ plane of figure 2, with a correspondence of points as shown.

Since $1 \leqslant \operatorname{sn}(\beta; l) \leqslant 1/l$ we have

$$\beta = K(l) - i\gamma \quad \text{for} \quad \gamma \quad \text{real and} \quad 0 \leqslant \gamma \leqslant K'(l). \tag{2.4}$$

It proves convenient to introduce a further variable, τ, by

$$\sigma = \operatorname{sn}(\tau; l), \tag{2.5}$$

so that the domain of variation of τ is the rectangle of figure 2. Then the transformation directly from τ to z is

$$\frac{z}{H} = \int_0^{\tau} \frac{\operatorname{cn}^2\tau\, d\tau}{1-l^2\operatorname{sn}^2\beta\operatorname{sn}^2\tau} = \tau - \frac{\operatorname{dn}\beta}{l^2\operatorname{sn}\beta\operatorname{cn}\beta}\Pi(\tau, \beta). \tag{2.6}$$

The elliptic integral $\Pi(\tau, \beta)$ is related to the theta and zeta functions of Jacobi by (Copson 1935, p. 408)

$$\Pi(\tau, \beta) = \tfrac{1}{2}\log\frac{\Theta(\tau-\beta)}{\Theta(\tau+\beta)} + \tau Z(\beta). \tag{2.7}$$

The physically given parameters s, t and g are related to the parameters H, l and β (or γ) of the mapping by rather complex expressions which we proceed to derive.

Near $\sigma = 1/l\,\mathrm{sn}\,\beta$ the mapping (2.3) behaves as

$$\frac{z}{H} \sim \frac{\mathrm{dn}\,\beta}{l^2\,\mathrm{sn}\,\beta\,\mathrm{cn}\,\beta}\log\left(\sigma - \frac{1}{l\,\mathrm{sn}\,\beta}\right)$$

and hence

$$\frac{s}{2H} = \frac{i\pi}{2}\frac{\mathrm{dn}\,\beta}{l^2\,\mathrm{sn}\,\beta\,\mathrm{cn}\,\beta}. \tag{2.8}$$

The point J has $z = \frac{1}{2}t$ and corresponds to $\tau = K$. Since $\Theta(\tau)$ is an even function of period $2K$ (Copson, p. 405), (2.7) implies that

$$\Pi(K, \beta) = KZ(\beta),$$

whence (2.6) implies

$$\frac{t}{2H} = K\left[1 - \frac{\mathrm{dn}\,\beta}{l^2\,\mathrm{sn}\,\beta\,\mathrm{cn}\,\beta}Z(\beta)\right]. \tag{2.9}$$

The point Q has $z = ig$ and corresponds to $\tau = iK'$. Using known properties of $\Theta(\tau)$ (Copson, pp. 405–406) we have

$$\frac{\Theta(iK' - \beta)}{\Theta(iK' + \beta)} = -\exp(i\pi\beta/K) = \exp(\pi\gamma/K),$$

so that (2.6) gives

$$\frac{g}{H} = K'\left[1 - \frac{\mathrm{dn}\,\beta}{l^2\,\mathrm{sn}\,\beta\,\mathrm{cn}\,\beta}Z(\beta)\right] + i\frac{\mathrm{dn}\,\beta}{l^2\,\mathrm{sn}\,\beta\,\mathrm{cn}\,\beta}\frac{\pi\gamma}{2K}. \tag{2.10}$$

Equations (2.8), (2.9) and (2.10) serve to determine H, l and $\beta = K - i\gamma$ in terms of s, t and g. Dividing (2.9) by (2.8) leads to

$$\frac{t}{s} = -\frac{2iK}{\pi}\left[\frac{l^2\,\mathrm{sn}\,\beta\,\mathrm{cn}\,\beta}{\mathrm{dn}\,\beta} - Z(\beta)\right]. \tag{2.11}$$

For a particular value of t/s, (2.11) relates β to l. Then (2.8), (2.9) and (2.10) combine to give

$$\frac{g}{s} = \frac{1}{2}\frac{K'}{K}\frac{t}{s} + \frac{1}{2}\frac{\gamma}{K}, \tag{2.12}$$

yielding the corresponding value of g/s. The mapping from the σ plane of figure 2 to the ζ plane of figure 1 is effected by

$$\sigma = \frac{1}{l\,\mathrm{sn}\,\beta}\,\mathrm{sn}\left(\frac{\zeta}{K(1/\mathrm{sn}\,\beta)}; \frac{1}{\mathrm{sn}\,\beta}\right),$$

and hence

$$\frac{1}{c} = \frac{K(1/\mathrm{sn}\,\beta)}{K'(1/\mathrm{sn}\,\beta)}, \tag{2.13}$$

leading to the couple for that particular value of g/s via (2.2). As $l \to 1$, then $\gamma \to 0$, $g/s \to 0$ and $G \to \infty$. As $l \to 0$, then $\gamma \to \infty$, $g/s \to \infty$ and $G \to 0$.

The particular geometry of interest for comparison with the experiments of part 1 has $t/s = \frac{1}{2}$. Writing this, and $\beta = K - i\gamma$, in (2.11), while changing the arguments of the elliptic functions to γ by the usual formulae, we get

$$Z(\gamma; l') - \frac{\mathrm{sn}\,(\gamma; l')\,\mathrm{dn}\,(\gamma; l')}{\mathrm{cn}\,(\gamma; l')} + \frac{\pi\gamma}{2KK'} + \frac{\pi}{4K} = 0. \tag{2.14}$$

A similar insertion in (2.12) leads to

$$\frac{g}{t+s} = \frac{1}{6}\frac{K'}{K} + \frac{1}{3}\frac{\gamma}{K}, \tag{2.15}$$

while (2.13) gives

$$\frac{(t+s)G}{\pi\mu\Omega R^4} = \frac{1}{c} = \frac{K(\mathrm{dn}(\gamma;l'))}{K'(\mathrm{dn}(\gamma;l'))}. \tag{2.16}$$

For $0{\cdot}05 \leqslant l^2 \leqslant 0{\cdot}95$, (2.14) was solved by interpolation and iteration via the tables of Milne-Thompson (1950). Then (2.15) and (2.16) gave the couple for the range of $g/(t+s)$ between 0·14 and 0·78, the tables of Eagle (1958) being used to determine K/K' where relevant.

Outside this range, interpolation from available tables to solve (2.14) becomes inaccurate, but asymptotic forms of the solution for large and small gaps can be obtained to cover the remaining values. While these can be derived by a limiting process on (2.14) it is instructive to consider a more direct approach.

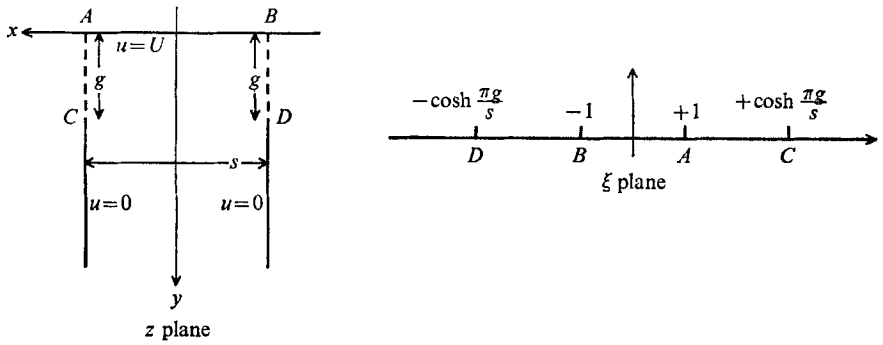

FIGURE 3. z plane and ξ plane for the asymptotic analysis with a small gap.

3. Asymptotic solution for a small gap

For small values of g in the z plane of figure 2 the dominant contributions to the force, F, arise from two separate regions. The narrow gap above the ridge of width t makes a contribution $\mu Ut/g$, while the contribution from above the groove may be estimated as equal to that for the case of infinitely thin plates ($t = 0$) sketched as the z plane in figure 3. This is the 'mathematical paint brush' treated by Taylor (1960), but with a non-zero gap.

This flow region is mapped by $\xi = \sin(\pi z/s)$ onto the upper half of the ξ plane, as shown in figure 3. The mapping onto the rectangle in the ζ plane of figure 1 via an elliptic function thus produces

$$\frac{1}{c} = \frac{K(q)}{K'(q)} \quad \text{where} \quad q = \mathrm{sech}\frac{\pi g}{s}.$$

Thus, for g small in the actual problem, we expect

$$F \sim 2\mu U\frac{K(q)}{K'(q)} + \frac{\mu Ut}{g}. \tag{3.1}$$

For the particular case $t/s = \frac{1}{2}$ this leads to

$$\frac{(t+s)\,G}{\pi\mu\Omega R^4} \sim \frac{K(q)}{K'(q)} + \frac{t+s}{g} \quad \text{where} \quad q = \operatorname{sech}\frac{3\pi g}{2(t+s)}. \tag{3.2}$$

For $g/(t+s) = 0{\cdot}14$ this agrees with the calculations from tables via (2.14) to better than 0·3 %, and hence was used for all lower values of g. In fact, for $l > 0{\cdot}9$ we have the asymptotic result

$$\frac{K(l)}{K'(l)} \sim \frac{2}{\pi}\left(\log\frac{4}{l'} - \frac{1}{4}l'^2\right), \tag{3.3}$$

to better than 0·3 %, and this too facilitates the computations.

4. Asymptotic solution for a large gap

For this limit we consider a shear flow over the grooves as shown in the z plane of figure 4. With $u = \operatorname{Re}\{\phi(z)\}$ we require $\phi(z) \sim -i\kappa z$ as $y \to +\infty$ for a shear of magnitude κ at large distances, while $u = 0$ on $CIJD$ and u takes equal values

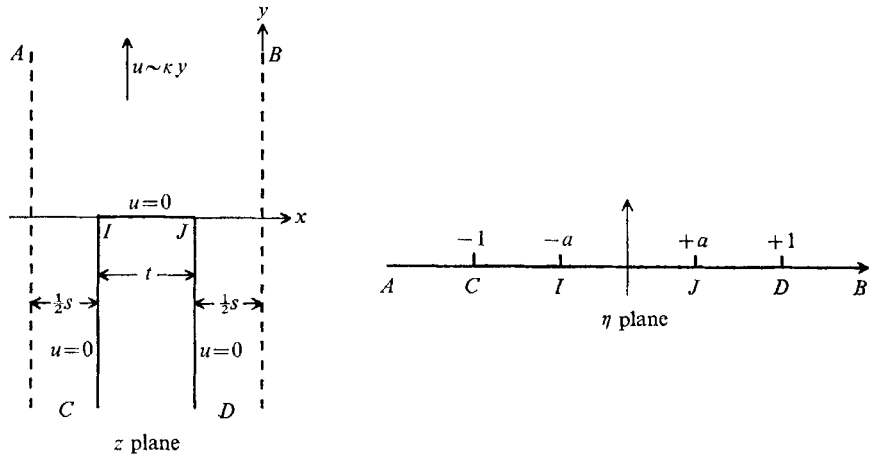

FIGURE 4. z plane and η plane for the asymptotic analysis with a large gap.

at points with equal ordinates on AC and BD. This flow region maps onto the upper half of the η plane of figure 4 by (Kober 1957),

$$\left.\begin{aligned} \frac{\pi}{t+s}z = \frac{\pi}{t+s}w(\eta) &= i\cosh^{-1}\frac{\eta}{a} - i\frac{(1-a^2)^{\frac{1}{2}}}{2}\cosh^{-1}\frac{\eta^2(2-a^2)-a^2}{a^2(\eta^2-1)} \\ \text{where} \qquad a &= \frac{(t^2+2ts)^{\frac{1}{2}}}{t+s}. \end{aligned}\right\} \tag{4.1}$$

The function $\chi(\eta) = \phi(w(\eta))$ has zero real part on CD, satisfies symmetry conditions on AC and BD, and

$$\chi(\eta) \sim \frac{t+s}{\pi}\kappa\log\eta \quad \text{as} \quad |\eta| \to \infty.$$

Thus

$$\chi(\eta) = \frac{(t+s)\,\kappa}{2\pi}\log\left(2\eta^2 - 1 + 2\eta\,(\eta^2-1)^{\frac{1}{2}}\right). \tag{4.2}$$

Expanding (4.1) and (4.2) for large $|\eta|$ we get the behaviour of $\phi(z)$ for large y as

$$\phi(z) \sim -i\kappa z + \frac{(t+s)\,\kappa}{2\pi}\left[(1-a^2)^{\frac{1}{2}}\log\left\{\frac{2-a^2+2(1-a^2)^{\frac{1}{2}}}{a^2}\right\}+2\log a\right], \tag{4.3}$$

to within exponentially small terms. The second term here is the slip velocity U_B discussed in part 1. In terms of s and t this is

$$U_B = \frac{\kappa}{2\pi}[t\log t+(t+2s)\log(t+2s)-2(t+s)\log(t+s)]. \tag{4.4}$$

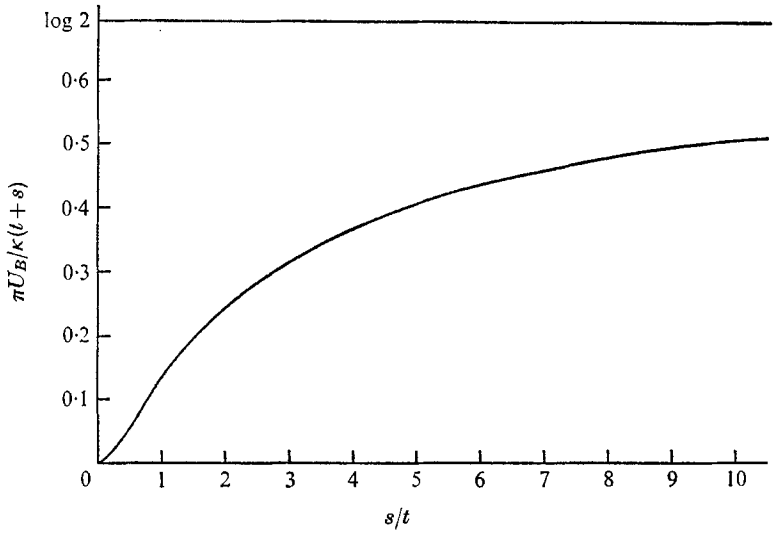

FIGURE 5. Variation of the slip velocity U_B for large gaps with the ratio s/t and the velocity gradient κ.

As $s \to 0$ (no grooves at all) we get $U_B \to 0$. As $t \to 0$ (plates of zero thickness) we get $U_B \to (s\kappa/2\pi)\log 2$. Since U_B is a physical quantity readily visualized, we plot, in figure 5, $\pi U_B/\kappa(t+s)$ as a function of s/t obtained from (4.4). Note that the limiting value of log 2 for $s/t \to \infty$ is attained incredibly slowly; at $s/t = 100$ its value is still 5 % away from the asymptotic value. Also, in the range $s/t = O(1)$, U_B shows a strong dependence on s/t.

For the particular value $t/s = \frac{1}{2}$ used previously, this result gives

$$U_B = 0{\cdot}07722\kappa(t+s).$$

For large g, the plate velocity is then asymptotically

$$U = \Omega r \sim \kappa g + U_B = \kappa[g+0{\cdot}07722(t+s)],$$

and the force per unit area on the plate is $\mu\kappa$. Integrating up to give the torque we reach

$$\frac{(t+s)\,G}{\pi\mu\Omega R^4} \sim \frac{1}{0{\cdot}1544+2g/(t+s)}. \tag{4.5}$$

For $g/(t+s) = 0{\cdot}78$ this agrees with the calculations from tables via (2.14) to better than 0·4% and hence was used for all higher values of g.

In this manner the curve of figure 4 of part 1 was plotted of $(t+s)\,G/\pi\mu\Omega R^4$ against $(t+s)/g$ over the whole range. For the case of plane parallel plates ($s = 0$) a similar plot gives a straight line of gradient $\frac{1}{2}$.

5. Boundary conditions at a porous surface

The assumption made by Beavers & Joseph (1967) is, in the present context,

$$\frac{U-U_B}{g} = \frac{\alpha}{k^{\frac{1}{2}}}\,U_B, \tag{5.1}$$

where k is the Darcy constant and α a dimensionless number which should depend only on the nature of the surface. For the particular model of a porous material adopted here,

$$k = \frac{s^3}{12(t+s)}. \tag{5.2}$$

The mean force per unit area on the plate is

$$\frac{F}{t+s} = \mu\,\frac{U-U_B}{g},$$

whence an integration yields

$$\frac{U-U_B}{U} = \frac{2g}{(t+s)}\,\frac{(t+s)\,G}{\pi\mu\Omega R^4}, \tag{5.3}$$

the ratio U_B/U being independent of the point on the disk. The quantity $(U-U_B)/U$ is plotted as a function of $g/(t+s)$ from (5.3) and the previously obtained data, in figure 5 of part 1 for the particular case $t/s = \frac{1}{2}$. It approaches unity for large gaps and $\frac{1}{3}(= t/(t+s))$ for small gaps.

From (5.1), (5.2), (5.3) and the previous data, it is a simple matter to compute the variation of α with g for the value $t/s = \frac{1}{2}$. This is shown in figure 6 of part 1; the asymptotic value of 2·035 is reached effectively at $g/(t+s) = 0{\cdot}5$, but α shows a rapid increase for lower values of g.

From the analysis of §4 it follows that the limiting value of α as $g \to \infty$ for general values of s/t is given by

$$\alpha \sim \frac{2\pi\,k^{\frac{1}{2}}}{t\log t + (t+2s)\log(t+2s) - 2(t+s)\log(t+s)}. \tag{5.4}$$

This variation of the asymptotic value of α with s/t is plotted in figure 7 of part 1. As $s/t \to 0$, we get $\alpha \to \infty$, while as $s/t \to \infty$ we get $\alpha \to \pi/3^{\frac{1}{2}}\log 4 = 1{\cdot}308$, this limit being attained rather slowly.

The author would like to thank Sir Geoffrey Taylor for providing the initial incentive for these calculations, and for many subsequent stimulating discussions. The work was carried out while in receipt of an I.C.I. Post-doctoral Research Fellowship.

Appendix

We here make an estimate of the errors introduced by assuming in the analysis that the grooves are infinitely deep. For this purpose, it is evident that the greatest error in estimating the actual stress at the moving plane occurs when

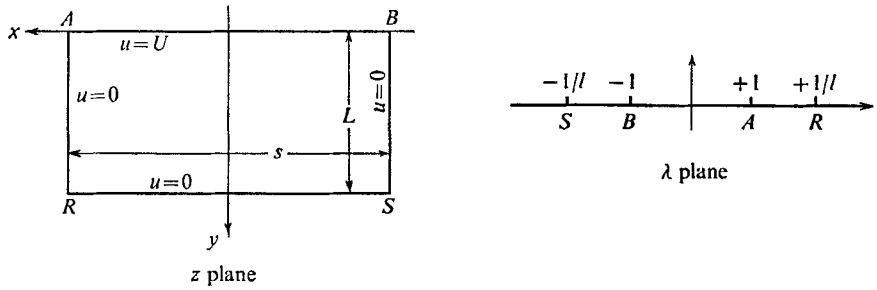

FIGURE 6. z plane and λ plane for the error estimation.

$g = 0$ and we therefore consider the problem sketched in the z plane of figure 6 in a rectangular channel of depth L, with $u \equiv \mathrm{Re}\{\phi(z)\} = U$ on AB, and $u = 0$ on $ARSB$. The mapping to the λ plane of figure 6 is effected by

$$\lambda = \mathrm{sn}\frac{2K(l)}{s}z \quad \text{where} \quad \frac{2L}{s} = \frac{K'(l)}{K(l)},$$

and in this plane the problem is solved by the function

$$\frac{U}{\pi i}\log\left(\frac{\lambda-1}{\lambda+1}\right),$$

so that we obtain the actual value of the velocity gradient on AB as

$$\left.\frac{\partial u}{\partial y}\right|_{y=0} = \frac{4U}{\pi}\frac{K(l)}{s}\left[\mathrm{dn}\frac{2K(l)}{s}x \Big/ \mathrm{cn}\frac{2K(l)}{s}x\right].$$

The approximation of $L \to \infty$ produces a result which may be derived as a limit of this, from §3 via the limit $g \to 0$, or from Taylor (1960), as

$$\left.\frac{\partial u}{\partial y}\right|_{y=0} \sim \frac{2U}{s}\sec\frac{\pi x}{s}.$$

Hence the ratio of the actual stress to the approximate stress is

$$\frac{2}{\pi}K(l)\cos\frac{\pi x}{s}\left[\mathrm{dn}\frac{2K(l)}{s}x \Big/ \mathrm{cn}\frac{2K(l)}{s}x\right].$$

This ratio is unity at $x = \pm\frac{1}{2}s$ and has a maximum of $(2/\pi)K(l)$ at $x = 0$. Thus a suitably simple estimate of the relative error, E, is provided by

$$E = \frac{2}{\pi}K(l) \quad \text{where} \quad \frac{L}{s} = \frac{1}{2}\frac{K'(l)}{K(l)}. \tag{A 1}$$

Certainly, the error in the force, F, and couple, G, obtained by integrating the stress must be less than this. For small l

$$K(l) \sim \tfrac{1}{2}\pi(1+\tfrac{1}{4}l^2+O(l^4)). \tag{A 2}$$

Using (3.3) and (A 2) we get

$$E = 1 + 4e^{-2\pi L/s} + O(e^{-4\pi L/s}). \tag{A 3}$$

In the actual experiment $L/s = 4$, so that the error is $O(4e^{-8\pi}) < 10^{-10}$, this value being well within the range of validity of the approximations (3.3) and (A 2). Thus the simplifications of infinite depth used in the calculations involve a negligible error.

REFERENCES

BEAVERS, G. S. & JOSEPH, D. D. 1967 *J. Fluid Mech.* **30**, 197.

CAYLEY, A. 1895 *An Elementary Treatise on Elliptic Functions*, 2nd edn. Bell & Sons (Dover reprint 1961).

COCKCROFT, J. D. 1927 *J. Inst. Elec. Engrs*, **66**, 385.

COPSON, E. T. 1935 *An Introduction to the Theory of Functions of a Complex Variable.* Oxford University Press.

EAGLE, A. 1958 *The Elliptic Functions As They Should Be.* Cambridge: Galloway & Porter.

KOBER, H. 1957 *Dictionary of Conformal Representations.* Dover.

MILNE-THOMSON, L. M. 1950 *Jacobian Elliptic Function Tables.* Dover. (Republished by Macmillan 1970.)

TAYLOR, G. I. 1960 *J. Fluid Mech.* **9**, 218.